Natural Resources for Human Health
eISSN: 2583-1194

Original Research

Received 02 July 2026
Revised 23 Aug 2026
Accepted 06 Sep 2026

Natural Resources for Human Health 2026, Vol. 6 (19s): 794–808

KEYWORDS:
Zinc oxide nanoparticles (ZnO NPs); Mentha extract; Antibacterial activity; Green synthesis.

Green Synthesis of ZnO Nanoparticles Using Mentha Extract: Physicochemical Characterization and Antibacterial Activity Against Staphylococcus aureus and Pseudomonas aeruginosa

Zainab K. Ali[1], Hind M. Al mossawey[2], Suhaila S. Mukhlif[3], Zina M. Tuaimah[4], Lubna A. Asmael[5], Omar M. Abdulbaqi[6], Ahmed A. Abdulhadi [7]

[*1]Scientific Research Commission, Baghdad, Iraq
Email: zainabalkhafaji@mohesr.edu.iq ORCID: 8398-2945-0000-0009
[*2]Scientific Research Commission, Baghdad, Iraq
Email: hind.m.ganoos@src.edu.iq ORCID: 0009-0002-8968-3743
[*3]Scientific Research Commission, Baghdad, Iraq
Email: suhaila1976@mohesr.edu.iq ORCID: 0009-0005-4976-935X
[*4]Scientific Research Commission, Baghdad, Iraq
Email: zinamohammad1980@gmail.com ORCID: 0009-0000-4594-1566
[*5]Scientific Research Commission, Baghdad, Iraq
Email: lubnaayad1978@gmail.com ORCID: 0009-0003-5053-3411
[*6]Scientific Research Commission, Baghdad, Iraq
Email: dromarlover@gmail.com ORCID: -5971-0001-0009-3676
[*7]Scientific Research Commission, Baghdad, Iraq
Email: ahmedbio8587@gmail.com ORCID: 0009-0004-2803-1674

ABSTRACT: This work describes a novel, quick, straightforward, green synthesizing methodology of zinc oxide nanoparticles (ZnO NPs) via mint leaf extract (Mentha) as a natural reducing and stabilizing agent. Characterization of nanoparticles was performed by Fourier-Transformed Infrared Spectroscopy (FTIR), X-ray Diffraction (XRD), and Scanning Electron Microscopy (SEM). FTIR findings showed that the bands at 480–500 cm^{-1} were assigned as Zn-O stretching vibrations, indicating the function of active compounds in reduction and stabilization where hydroxyl and phenolic groups are involved during the process. XRD results suggested crystallization of ZnO as a single phase, with clear evidence that the hexagonal wurtzite structure was obtained, showing no extra phases. The SEM images showed that the ZnO NPs had a predominantly quasi-spherical shape, with a slight tendency to aggregate. The agar diffusion method was used to determine the antibacterial activity of synthesized ZnO NPs against Staphylococcus aureus and Pseudomonas aeruginosa, respectively. This antibacterial effect may be attributed to multiple mechanisms proposed in previous studies, including the possible generation of reactive oxygen species (ROS), which can contribute to oxidative cellular damage and bacterial cell membrane disruption. In conclusion, these results indicate that there is a strong relationship between nanoparticle structures and their antibacterial capability. In this regard, the current work demonstrates a cost-effective and green synthesis pathway coupled with knowledge of microbial activity-influencing factors.

Natural Resources for Human Health
eISSN: 2583-1194

INTRODUCTION

Antimicrobial resistance (AMR) has become a growing threat to public health worldwide, with AMR leading to a reduction in the clinical effectiveness of many commonly used antibiotics. Pseudomonas aeruginosa and Staphylococcus aureus are among the most troublesome pathogens: both species can evolve and harbor multiple mechanisms of resistance. (Baruah *et al.,* 2024). Pseudomonas aeruginosa is a Gram-negative bacterium that has intrinsic resistance mechanisms such as reduced membrane permeability, the presence of active efflux pumps, and biofilm formation. S. aureus, a Gram-positive organism which is often associated with severe infections as well as the emergence of methicillin-resistant strains (MRSA) significantly reduces host defenses. (Wu *et al.* (2024). These fundamental variations in cell wall structure and physiology between Gram-positive (GP) and Gram-negative occur as differences in response to antimicrobial agents, indicating the need for alternative techniques with activity against a broad range of bacterial pathogens (Davati and Ghorbani, 2024). One such hope against the battle of antimicrobial resistance is nanotechnology, and more on it can be explored in this scenario. So, in particular ZnO NPs have been extensively studied with respect to their excellent bactericidal properties and also those of the stability and relative nontoxicity (Bisht et al., 2024; Nan *et al.,* 2024). Antimicrobial activity is not mediated via a defined mechanism but occurs through multiple mechanisms including generation of reactive oxygen species (ROS), Zn^{2+} release, and direct interaction with bacterial cell membranes. (Zubair *et al.* 2025). Collectively, these effects can create oxidative distress, leading to death of bacterial cells and thereby giving ZnO NPs strong antibacterial activity against many microorganisms (Riahi *et al.* 2023). In recent times, there is increasing interest in sustainable green approaches for the synthesis of nanoparticles. Green synthesis by using plant extracts offers a sustainable alternative to traditional chemical methods, with minimal uses of toxic reagents (El-Saadony *et al.,* 2024). Hence, extracts from Mentha species are especially ideal for this because of high levels of phenolics and flavonoids, bioactive compounds (Nasir *et al.,* 2026). These compounds can act as both natural reducing and stabilizing agents optimized for nanoparticle production through two different processes' ability to give flexibility with tunable surface properties (Kamal *et al.* 2024). Consequently, green-produced ZnO nanoparticles usually exhibit improved biological activity and bioavailability with more dispersion and reduced toxicity relative to those prepared by conventional methods (Rajalakshmi *et al.,* 2026). Despite these advances, many previous studies have tended to focus either on nanoparticle synthesis and characterization or on antibacterial evaluation as separate aspects (Al-Darwesh *et al.,* 2024; Laskar & Saha, 2025). Moreover, few studies combining comprehensive physicochemical characterization (e.g., functional groups (FTIR), crystallinity (XRD) and morphology (SEM)) with systematic evaluation of antibacterial activity are available. This caveat prevents a direct insight for how structural features might correlate to bioactivity and further complicated by the fact that such comparisons are across different classes of bacteria. (Udayagiri, 2024). This study aims to bridge the aforementioned research gap by synergistically combining green synthesis with systematic characterization and in vitro antibacterial evaluation. ZnO nanoparticles were prepared using Mentha extract as natural reducing and stabilizing agents, then their structural and morphological properties were analyzed extensively by FTIR, XRD, and SEM techniques. (Dar *et al.,* 2025). Their antibacterial activity was then evaluated against Staphylococcus aureus and Pseudomonas aeruginosa in order to explore the relationship between nanoparticle characteristics and antimicrobial performance (Mazumder *et al.,* 2024; Rad *et al.,* 2019).

MATERIALS AND METHODS

Materials

Zinc acetate dihydrate ($Zn(CH_3COO)_2 \cdot 2H_2O$), fresh mint leaves (Mentha sp.), sodium hydroxide (NaOH), distilled water, and ethanol (when required) were used throughout the study without further purification.

Preparation of Mint Leaf Extract

The fresh mint leaves were first washed with tap water to remove surface impurities and then rinsed with distilled water. In a shade condition, the cleaned leaves were dried at room temperature for 3–5 days. Then air-dried and finely powdered. Powder (10 g) was transferred to 100 mL distilled water and subjected to heating at 60–70 °C with stirring for about 45 min. The mixture was cooled to room temperature and filtered through Whatman No. 1 filter paper. The extract was kept at 4°C, and this can be used for the next 48 h without loss of activity **(**Xu *et al.,* 2021).

Preparation of Zinc Acetate Solution

The solution is 0.25 M of zinc acetate dihydrate (5.5 g in 100 mL distilled water). Prior to use, the solution was heated to 60 °C to ensure complete dissolution and obtain a homogeneous solution **(**Zeghoud *et al.,* 2022).

Green Synthesis of ZnO Nanoparticles

In order to synthesize the nanoparticles, 50 mL of the prepared mint extract was added dropwise to zinc acetate solution with stirring at a constant temperature (60–70°C) over a period of several minutes (in small increments every 2–3 min). Next, 1 M NaOH was added dropwise to adjust the pH of the mixture to 9–10. The reaction was carried out with stirring for 2–3 h. The formation of a nano-precipitate of ZnO occurred by producing either a milky whitish precipitate (Al Sharif *et al.,* 2025).

Separation, Purification, and Calcination

The homogeneous reaction mixture was then incubated at room temperature for 12–24 hours to allow full precipitation. For those with a more intense finish, the obtained precipitate was harvested by centrifugation at 8000 rpm for 15 minutes. Then, it was washed multiple times with distilled water and a last wash with ethanol to ensure that no pollutant remained. It was followed by drying of the purified product at 60–80°C for 12 h. Thereafter, the resulting dried powder was calcined to form some amount of crystalline ZnO nanoparticle at a temperature ranging from 400–450° C for 2 hours. The cooled product was taken in air-tight containers for further studies. It is worth noting that controlled addition of the plant extract and careful pH adjustment were critical factors in achieving better yield and uniformity of the nanoparticles **(**Mutukwa *et al.,* 2024).

Preparation of Culture Media

Sensitivity of bacterial strains to different antibiotics Nutrient agar (NA) medium was prepared according to the manufacturer's directions where we dissolve required quantities in distilled water. The medium was autoclaved at 121°C for 15 minutes at a pressure of 15 psi. It cooled to 45–50°C after sterilization and was distributed (20 mL each plate) on sterile Petri dishes under aseptic conditions. These plates were allowed to set to solid and kept at 4°C for further use **(**Sharma *et al.,* 2017).

Bacterial Strains and Inoculum Preparation

One Gram-positive strain (Staphylococcus aureus) and one Gram-negative strain (Pseudomonas aeruginosa) were chosen for this study. The bacterial strains were obtained from authorized laboratory sources and were officially provided by the Research and Technology Center for Environment, Water, and Renewable Energy. The use of these bacterial strains was reviewed and approved by the Research Ethics Committee of the Center for Processing and Disposal of Chemical, Biological, and War Waste (Ref. No. SRC/58/0015, October 15, 2025). The bacterial strains were subcultured on nutrient agar plates and incubated at 37°C for 18-24 h. Subsequently, the fresh-grown bacterial colonies were collected suspended in sterile normal saline (0.85% NaCl). The turbidity of the bacterial suspension was adjusted to 0.5 McFarland standard, corresponding to approximately 1 x 10^8 CFU/mL, to ensure a standardized bacterial inoculum for all antibacterial activity assays. (Wicks *et al.,* 2022).

Inoculation of Plates (Lawn Culture Method)

To obtain a uniform bacterial lawn, 0.1 mL of the prepared culture was streaked across the surface of nutrient agar plates using a sterile cotton swab. The plates were placed undisturbed for 10–15 min to absorb excess moisture (Sanders, 2012).

Agar Well Diffusion Assay

The agar well diffusion method was used to assess the antibacterial activity of the synthesized ZnO nanoparticles. A stock suspension of 100 mg/mL was prepared by dispersing 1.5 g of the synthesized powder ZnO nanoparticle in 15 mL of sterile distilled water. This undiluted suspension was taken as the 100% stock concentration. Two-fold dilutions were then prepared to obtain concentrations of 50%, 25%, 12.5%, 6.25%, and 3.125% for evaluating antibacterial activity against the Gram-positive and Gram-negative bacterial strains included in this study. Using a sterile cork borer, wells of approximately 6 mm in diameter were aseptically formed on the agar plates containing microbial growth. Each well was loaded with 50–100 µL of the appropriate ZnO nanoparticle suspension. Reproducibility and reliability of the results were confirmed by triplicate experiments for all data (Balouiri *et al.,* 2016).

Incubation

Natural Resources for Human Health
eISSN: 2583-1194

The inoculated plates were incubated in an inverted position at 37°C for 24 h. under appropriate conditions (Duque-Sanchez *et al.,* 2024).

Measurement of Inhibition Zones

A digital ruler or a Vernier caliper with an accuracy of millimeters was used to measure the diameteres of the inhibition zones formed around each well after incubation. The diameter of the well (well diameteres) was measured and recorded, and for each concentration, the average value from three independent readings was calculated. (Chandrasekar *et al.,* 2015).

RESULTS

FTIR Analysis

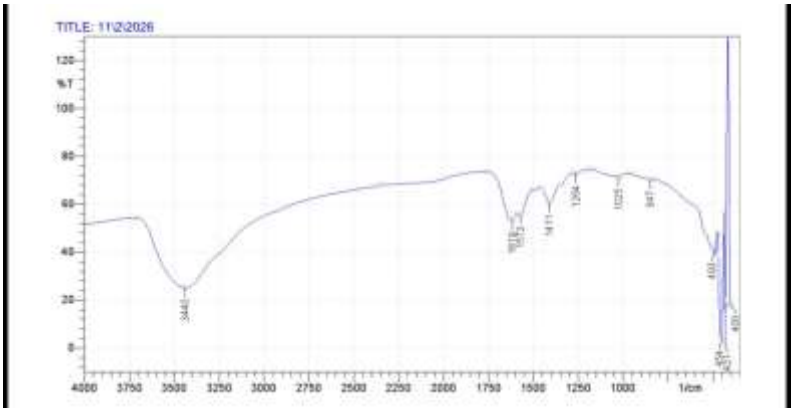


Figure 1: FTIR spectrum of the synthesized ZnO nanoparticles showing characteristic absorption bands, including a broad O–H stretching peak around 3440 cm^{-1} and a distinct Zn–O vibration band in the region below 500 cm^{-1}, confirming nanoparticle formation.

The FTIR spectrum observed from 4000–400 cm^{-1} revealed a prominent broad absorption band around 3439 cm^{-1} Other bands of absorption at 1619 cm^{-1} and 1573 cm^{-1} were also observed. Several peaks in the band region 1200–1000cm−1(1264, 1025&847cm−1)were observed. At lower wavenumbers, below 500 cm^{-1} (around 493–400 cm^{-1}), additional absorption bands , which was also detected. A detailed examination of peaks listed in the table confirmed the presence of 11 absorption peaks, with variations in their position, intensity, width, and peak area.

XRD Analysis

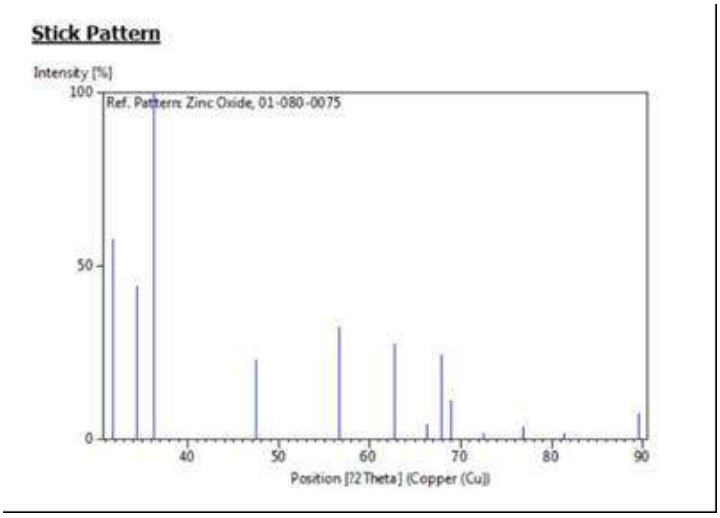


Figure 2: XRD pattern confirming the crystalline structure and successful formation of ZnO nanoparticles.

X-ray diffraction (XRD) results showed diffraction peaks corresponding to the hexagonal wurtzite structure of zinc oxide (ZnO). The calculated lattice parameters (a = b ≈ 3.25 Å and c ≈ 5.21 Å) along with the space group $P6_3mc$ are in very good accordance with respect to those reported for ZnO comparing to the standard crystallographic data available from well-known literature reporting structural studies such as those performed by Ümit Özgür et al. (2005). The positions of clearly defined diffraction peaks at (100), (002), and (101) are around ~31.7°, 34.4°, and 36.2° for ZnO, respectively, from the diffraction pattern.

Dislocation density ($\times10^{15}$ lines/m^2)	**Microstrain$\times10^{-3}$**	**Crystallite size, (nm)**	**FWHM (°)**	**2θ (°)**	**Plane**
1.87	2.77	23.1	0.3581	31.71	(100)
1.29	2.10	27.8	0.2996	34.36	(002)
1.74	2.33	24.0	0.3476	36.20	(101)
1.63	**2.40**	**25.0**	**----**	**----**	**Average**

Table (1): Crystallite size, microstrain, and dislocation density of the biosynthesized ZnO nanoparticles calculated from the XRD diffraction peaks using the Debye-Scherrer equation.

The crystallite size of the synthesized ZnO nanoparticles was estimated using the Debye-Scherrer equation based on the most intense diffraction peaks ((100), (002), and (101)). The calculated crystallite sizes ranged from 23.1 to 27.8 nm, with an average crystallite size of approximately 25.0 nm. In addition, the lattice microstrain and dislocation density were calculated from the XRD peak broadening to evaluate the crystal defect structure. The obtained values indicate good crystallinity with a moderate defect concentration, which may contribute to the enhanced antibacterial performance through facilitating ROS generation.

SEM Analysis

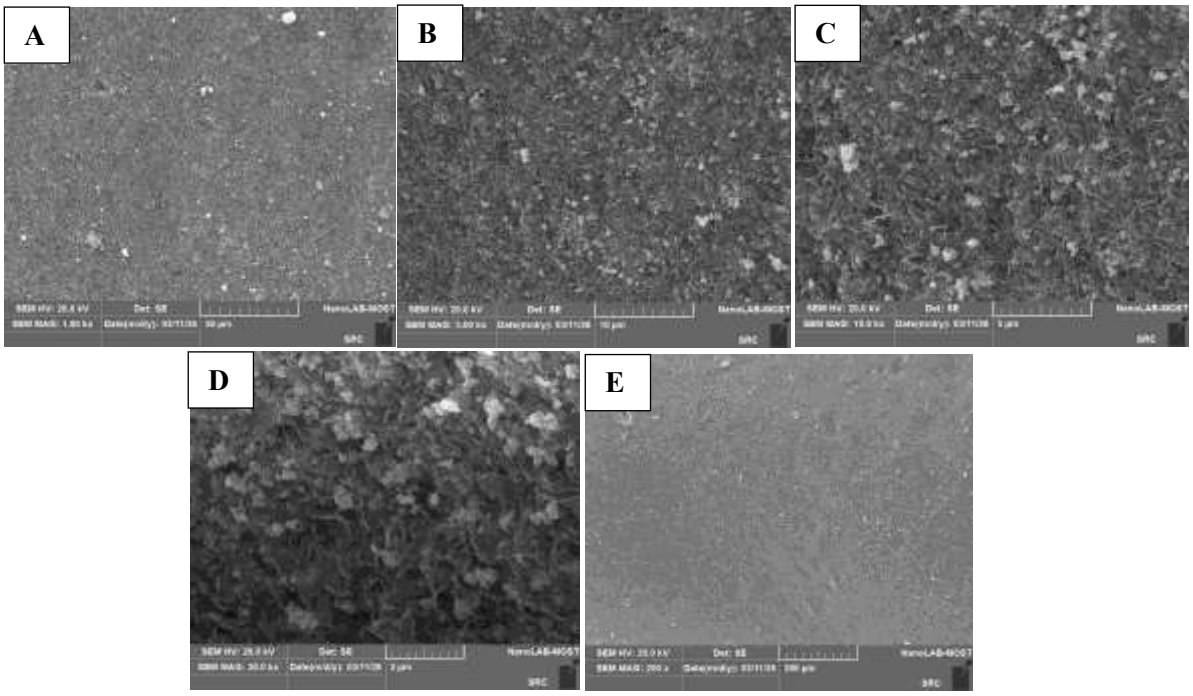


Figure 3: A. SEM image showing a relatively uniform surface morphology with fine particle distribution and slight agglomeration (scale bar: 50 μm). B. SEM image showing dense particle distribution with noticeable agglomeration and increased surface roughness (scale bar: 10 μm). C. SEM image showing highly aggregated fine particles with irregular morphology and pronounced surface roughness (scale bar: 5 μm). D. SEM image of green-synthesized ZnO nanoparticles showing aggregated, irregularly shaped particles with porous surface morphology at a scale of 2 μm. E. SEM image (200×) showing a relatively uniform surface morphology with fine particle distribution and minimal agglomeration, indicating successful formation of ZnO nanoparticles.

The SEM micrographs revealed a relatively compact and uniform surface composed of closely packed granular particles with irregular morphology. At lower magnification (200×), the surface exhibited an uneven particle distribution with micro-scale roughness, together with small aggregates and sporadic deposits. No deep voids or significant cracks were observed, indicating that the material remained structurally continuous and relatively homogeneous. Some regions exhibited brighter contrast, which may be attributed to electron scattering or variations in surface topography. At higher magnification (5.00 k×), the morphology became more distinct, revealing a densely packed and highly agglomerated network of nanoparticle clusters. The particles formed interconnected aggregates composed of fine granules, while individual nanoparticles could not be clearly distinguished because of strong interparticle interactions, including the high surface energy and van der Waals forces associated with nanomaterials. The observed particle size ranged predominantly from the nanoscale to the submicron scale. A few striated or linear surface features were also observed, which may represent artifacts introduced during sample preparation or intrinsic structural characteristics. Overall, the SEM observations confirmed the successful formation of nanostructured ZnO with a rough and a moderate degree of nanoparticle agglomeration and heterogeneous surface . This morphology is characteristic of green-synthesized ZnO nanoparticles, where rapid nucleation followed by spontaneous particle aggregation leads to the formation of densely packed nanoparticle clusters. Such agglomeration is commonly observed in nanomaterials as a consequence of surface energy minimization.

Antibacterial activity

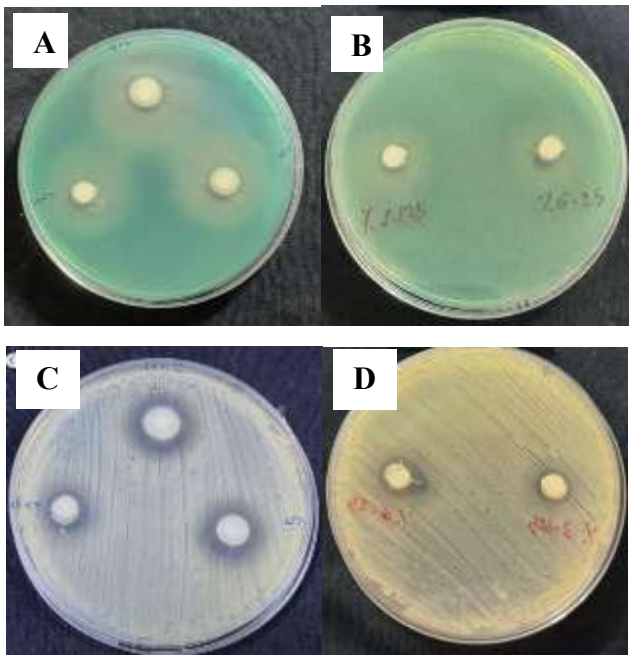


Figure 4. Zones of inhibition produced by green-synthesized ZnO NPs at varying concentrations against target pathogens: (A, B) Dose-dependent inhibition against Gram-negative Pseudomonas aeruginosa across concentrations (50%, 25%, 12.5%, 6.25%, and 3.125%), (C, D) Dose-dependent inhibition against Gram-positive Staphylococcus aureus across concentrations (50%, 25%, 12.5%, 6.25%, and 3.125%).

Natural Resources for Human Health
eISSN: 2583-1194

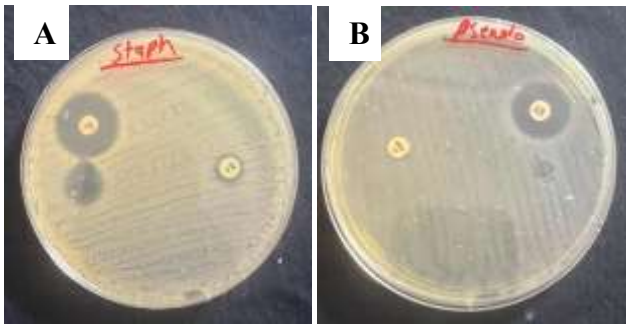


Figure 5. Control plates for antibacterial assays: (A) Staphylococcus aureus exposed to Gentamicin standard disk (CN 10) and negative control, (B) Pseudomonas aeruginosa exposed to Piperacillin/Tazobactam standard disk (TZP 110) and negative control.

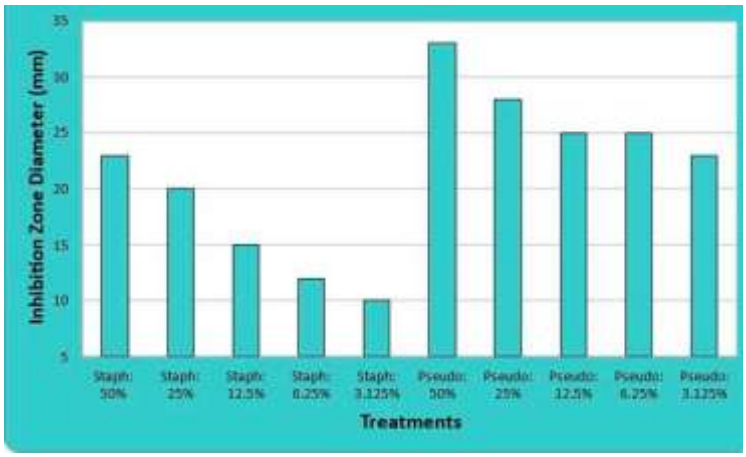


Figure 6. Relationship between concentration of ZnO Nanoparticles

Inhibition Zone Diameter of Staphylococcus aureus and Pseudomonas aeruginosa.

The antibacterial activity of the biosynthesized ZnO nanoparticles was evaluated against Pseudomonas aeruginosa and Staphylococcus aureus using the agar well diffusion method. , the nanoparticles exhibited a clear concentration-dependent antibacterial effect against both bacterial strains, with nanoparticle concentration increasing as inhibition zones increased. Pseudomonas aeruginosa was more susceptible to the ZnO nanoparticles than Staphylococcus aureus. The largest inhibition zone against Pseudomonas aeruginosa was 33.00 ± 2.16 mm at the 50% concentration, while inhibition remained relatively high at the intermediate concentrations of 25% and 12.5%, measuring 28.00 ± 1.09 mm and 25.00 ± 1.64 mm, respectively. In contrast, the maximum inhibition zone against Staphylococcus aureus was 23.00 ± 1.41 mm at the 50% concentration, gradually decreasing to 10.00 ± 0.54 mm at the lowest tested concentration (3.125%). The nanoparticles retained measurable antibacterial activity even at the lowest concentration tested. The agar plate images were consistent with these findings, showing larger and more distinct inhibition zones at higher nanoparticle concentrations, particularly against Pseudomonas aeruginosa, as shown in (Fig.4. A,B,C,D). additionally, standard controls were evaluated to validate the assay, the negative controls exhibited no zone of inhibition against either bacterial strains, confirming the absence of intirinsic antibacterial activity from the solvent. In contrast, the positive control antibiotics demonstrated distinct clear zones of inhibition, with gentamicin (CN 10) producing a pronounced clear zone against Staphylococcus aureus and piperacillin/tazobactam (TZP 110) showing effective antibacterial inhibition against Pseudomonas aeruginosa (Fig. 5. A and B). Statistical analysis using the least significant difference (LSD) test indicated that the differences among treatments were highly significant ($P \leq 0.01$), confirming that the observed variations in antibacterial activity were primarily attributable to nanoparticle concentration rather than random variation (Fig. 6).

Pesudomonas aereginosa (mm) Mean ± SD	Staphylococcus aureus (mm) Mean ± SD	ZnO NP concentration (%)
32.67 ± 0.58	22.67 ± 0.58	50
28.33 ± 0.58	19.33 ± 0.58	25
24.33 ± 0.58	15.33 ± 0.58	12.5
24.33 ± 1.15	12.33 ± 0.58	6.25
23.33 ± 0.58	9.33 ± 0.58	3.125
—	32.33 ± 0.58	Positive control gentamicin (10µg)
17.33 ± 0.58	—	Positive control piperacillin/tazobactam (100/10µg)
0.00 ± 0.00	0.00 ± 0.00	Negative control sterile distal water
Values are expressed as mean ± standard deviation (SD) three independent experiments (n=3). The symbol (—) indicates that The specific antibiotic disk was not evaluated against that strain.		

Table (2): Antibacterial activity (Zone of Inhibition in mm) of ZnO NPs and standard controls against S. aureus and P. aeruginosa.

The antibacterial activity of the synthesized zinc oxide nanoparticles (ZnO NPs) was evaluated using the agar well diffusion assay against Staphylococcus aureus and Pseudomonas aeruginosa. The mean all test concentrations and reference controls are presented in (Table 2). the ZnO NPs exhibited a dose-dependent antibacterial effect against both bacterial strains. For Staphylococcus aureus, the highest concentration (50%) produced a mean inhibition zone of 22.67 ± 0.58 mm, which gradually decreased with lower concentrations to 19.33 ± 0.58 mm (25%), 15.33 ± 0.58 mm (12.5%), 12.33 ± 0.58 mm (6.25%), and 9.33 ± 0.58 mm (3.125%). The positive control gentamicin (10 µg) showed a mean inhibition zone of 32.33 ± 0.58 mm. Similarly, for Pseudomonas aeruginosa, the ZnO NPs displayed inhibition zones measuring 32.67 ± 0.58 mm (50%), 28.33 ± 0.58 mm (25%), 24.33 ± 0.58 mm (12.5%), 24.33 ± 1.15 mm (6.25%), and 23.33 ± 0.58 mm (3.125%). The positive control Piperacillin/Tazobactam (100/10 µg) yielded an inhibition zone of 17.33 ± 0.58 mm. The negative control sterile distal water, showed no antibacterial activity (0.00 ± 0.00) against either strain (Table 2).

DISCUSSION

FTIR Analysis

This observation is consistent with well-known observations that hydrogen-bonded hydroxyls give rise to broad absorptions in the region of 3200–3600 cm^{-1} (Al-Amin *et al.,* 2025). This kind of characteristic shows that hydroxyl-containing species, alcohols & phenols, or water adsorbed on the surface remains. However, the wide peak could not be correlated only to structural hydroxyl groups' content; the presence of moisture or intermolecular hydrogen bonding might also affect the position and appearance of the band. (Hsiao *et al.,* 2025). These assignments are in line with typical FTIR reference data, where such vibrations generally appear between 1500 and 1700 cm^{-1} (Talukdar *et al.,* 2024). Considering the phytochemical composition of Mentha extract, these aromatic-related vibrations may be associated with phenolic compounds such as rosmarinic acid and flavonoids, which contain aromatic rings together with hydroxyl and other oxygen-containing functional groups. These compounds may have participated in the formation of ZnO nanoparticales by interacting with zinc species during the synthesis and subsequently becoming associated with the nanoparticale surface, thereby contributing to surface capping and stabilization (Laskar & Saha, 2025). This qualitative interpretation is consistent with the reported spectral behavior of C–O bonds. Such oxygen-containing groups can plausibly originate from Mentha phytochemicals, particularly phenolic compounds and flavonoids, while the hydroxyl group of menthol may also contribute to interactions with the ZnO surface. Therefore, menthol may have participated mainly in surface capping through its hydroxyl functionality, whereas rosmarinic acid and flavonoids, owing to their multiple hydroxyl and oxygen-containing groups, are considered more likely to contribute substantially to the coordination and stabilization of the ZnO nanoparticles (Bisht et al., 2024). This could imply the existence of inorganic materials, as more or less this feature has been found within investigations focused on metal oxides and lattice vibrations. (Shukla, 2025).. Overall, the FTIR findings indicate that Mentha-derived phytochemicals, particularly rosmarinic acid, flavonoids, and possibly menthol, may have played complementary roles in the green synthesis of ZnO NPs, with their oxygen-containing functional groups contributing to the interaction with zinc species and the subsequent capping and stabilization of the nanoparticles. However, these assignments should be considered as plausible hypotheses, since FTIR

alone cannot definitively identify the contribution of an individual phytochemical or establish its specific role in the reduction and capping processes (Sahithya et al., 2022).

XRD Analysis

The evidence of the crystalline nature is clear from the X-ray diffraction (XRD) patterns showing the hexagonal wurtzite structure of zinc oxide (ZnO). Comparison with existing x-ray crystallography data supports this interpretation well (Mansy *et al.,* 2023). The observed crystal structure is consistent with the characteristic hexagonal wurtzite structure of ZnO reported in the literature (Verma, L.M., et al. (2024)). characteristic diffraction reflections of ZnOcan indicate an element of preferred orientation or anisotropic growth dependent upon synthesis parameters, including temperature, precursor concentration, and pH conditions (Zak *et al.,* 2024). Furthermore, the broadening of the most intense (101) diffraction peak was used to estimate the microstrain and dislocation density of the synthesized ZnO nanoparticales. Based on the observed FWHM of 0.34760° at $2\theta = 36.1978°$, the microstrain (ε) was calculated using the Stokes-Wilson relation, $\varepsilon = \beta/(4\tan\theta)$, where β is the FWHM in radians and θ is the Bragg angle. The calculated microstrain was 4.64×10^{-3}. The crystallite size estimated from the same (101) peak using the Debye-Scherrer equation was 24.04 nm, and the corresponding dislocation density (δ), calculated from $\delta = 1/D^2$, was 1.73×10^{15} m^{-2}. These values indicate the presence of a measurable degree of lattice distortion and crystal defects within the ZnO nanocrystals. Such structural defects can influence the surface reactivity and electronic properties of ZnO and may contribute to reactive oxygen species (ROS) generation, which is relevant to the antibacterial activity of the synthesized nanoparticles (Jabeen, S. (2020). A further remark is that the diffraction peaks observed do not show any additional peaks indicating that there are no additional secondary phases or impurities detected in the detection limits of this technique. aligning with previous literature on similar systems (Tran *et al.,* 2024). Although the XRD results confirmed the successful formation of phase-pure crystalline ZnO, this technique primarily provides information on the crystal phase and crystalline structure. Therefore, SEM analysis was performed to further investigate the surface morphology and distribution of the synthesized nanoparticles (Khorsand Zak and Hashim, 2025). Therefore, the XRD data provide strong evidence for the formation of phase-pure zinc oxide (ZnO); SEM characterization complements these findings by providing detailed information on the particle distribution and surface morphology of the synthesized nanoparticles (Kuryliszyn-Kudelska and Dobrowolski, 2026).

SEM Analysis

The surface morphology shown in (Fig. 3A) suggests the formation of a relatively compact and uniform nanostructured material. The absence of visible cracks and the overall homogeneity of the surface are consistent with reports describing controlled synthesis approaches, where gradual nucleation and growth tend to produce densely packed structures with fewer defects (Xie *et al.,* 2026). At the same time, the presence of particle agglomeration is not unexpected, particularly for ZnO-based nanomaterials, as nanoparticles with high surface energy tend to cluster during drying or subsequent heat treatment. Localized compositional differences or electron density variations may cause brightness variation across the image, but topography can also be responsible for generating contrast (Chen *et al.,* 2022). At higher magnification, regional motifs allow morphology to become more clearly defined (Fig. 3B) as a densely agglomerated structure revealing an obviously rough surface. This observation is consistent with the expected behavior of nanomaterials, where attractive interparticle forces (primarily van der Waals) drive aggregation in the absence of stabilizing agents (Lee *et al.,* 2023). The observed roughness and heterogeneity in surface topography indicate a highly irregular surface; however, surface area cannot be reliably inferred from SEM morphology alone (Sahithya et al. (2022). It is important to be aware that features such as these can be affected by post-synthesis processing, including drying conditions (Babaei and Bazyari, 2022). The image in (Fig. 3C), at an even greater magnification, shows a tightly interconnected meshwork of sub-micrometer-sized irregularly shaped particles. It looks like a dense structure with units aggregated in a porous-like manner at the nanoscale level. Such morphology is frequently observed in chemical or thermal procedures to synthesize nanomaterials, where nucleation occurs rapidly followed by particle growth and subsequently aggregation (Nguyen *et al.,* 2023). Such bright areas within the image may indicate differences in local composition or electron scattering tendency. However, the effective porosity and aggregation should be interpreted with caution since they may be partly influenced by sample preparation artifacts like clustering (induced by drying) or beam-induced alteration during imaging (Arat *et al.,* 2024). Because of the pronounced aggregation observed in the SEM images, the primary particle size cannot be determined reliably from SEM alone. Therefore, the numerical crystallite size was estimated from the broadening of the XRD (101) reflection using the Debye-Scherrer equation, yielding a crystallite size of

24.04 nm (Bisht et al. (2024). In (Fig. 3D), the ZnO nanoparticles show a non-uniform, highly aggregated morphology with irregularly shaped clusters distributed in a network configuration at a micrometer level. This morphology is frequently found in green synthesis methods, where bioactive compounds function as reducing and stabilizing agents. Though these compounds facilitate nanoparticle formation, they cannot always provide sufficient stabilization to prevent agglomeration (El Faroudi *et al.,* 2023). Furthermore, the particle coalescence step can be promoted by thermal treatment steps and thus participate in the formation of such structures. Although aggregation may reduce the accessible surface area of individual nanoparticles, interconnected agglomerates may still provide accessible external surfaces for interaction with the surrounding medium (Jabeen et al., 2020) . Finally, (Fig. 3E) displays an irregular surface with features such as particulate residues, linear gouges, and localized cracking. This morphology is likely a result of both intrinsic material properties and external effects such as mechanical stress, dehydration, or sample handling processes (Ali *et al.,* 2023). Preparation artifacts, from the coating processes or residual contaminants, can also lead to surface irregularities and particle accumulation. Differences in brightness across the image appear to be driven by differences in surface topography and electron emissions. Therefore, these brightness variations should not necessarily be interpreted as compositional differences (Ilett *et al.,* 2020). In conclusion, the SEM observations show an aggregated nanostructure with a rough and irregular surface, which is consistent with the morphology commonly reported for green-synthesized ZnO nanoparticles (Ali *et al.,* 2023).The pronounced agglomeration observed by SEM also explains why SEM was not used to assign an exact primary particle size; instead, the crystallite size was quantitatively determined from XRD with a value of 24.04 nm.

Antibacterial Activity

The antibacterial activity of the green-synthesized ZnO nanoparticles can be attributed to several complementary mechanisms. Among them, the generation of reactive oxygen species (ROS), including superoxide anion, hydroxyl radical, and hydrogen peroxide, is one of the main factors. (Jiang and Cai, 2020). Such reactive species can generate oxidative stress in the bacterial cell, which causes membrane damage, protein denaturation, and genetic material disruption. Also, the release of Zn^{2+} ions has an additional effect by disrupting the essential enzymatic processes and disrupting cell homeostasis (Vitasovic *et al.,* 2024). Additionally, the antibacterial activity is proposed to be affected by other physicochemical properties of the nanoparticles, like small size, large surface area, and crystalline nature, along with the presence of bioactive compounds from Mentha extract as revealed by previous characterization analyses. (Alavi *et al.,* 2020). However, the severe agglomeration observed in the SEM images may have negatively influenced the antibacterial performance of the synthesized ZnO nanoparticles. The formation of sub-micron clusters can reduce the effective surface area available for interaction with bacterial cells and may limit the accessibility of active ZnO surfaces (Sirelkhatim *et al.,* 2015; Lallo da Silva *et al.,* 2019). Consequently, agglomeration may reduce the contact between the nanoparticles and bacterial membranes and may also restrict the dissolution and release of Zn^{2+} ions from the accessible particle surfaces (Ahmed *et al.,* 2019). In addition, reduced surface accessibility may influence ROS generation at the nanoparticle-bacterium interface, potentially decreasing the overall oxidative stress imposed on bacterial cells. Therefore, although the synthesized ZnO nanoparticles retained measurable antibacterial activity, the observed agglomeration may have limited their maximum antibacterial efficacy (Sirelkhatim *et al.,* 2015; Mendes *et al.,* 2022). This effect may explain why the biological activity does not necessarily reflect the full intrinsic antibacterial potential expected from well-dispersed ZnO nanoparticles (Lallo da Silva *et al.,* 2019; Jabeen *et al.,* 2024). Although P. aeruginosa showed greater sensitivity in this case, Gram-negative bacteria are often thought to be more resistant because of the presence of an outer layer made up of lipopolysaccharides that can act as a barrier to external agents (Xu *et al.,* 2026). However, this is not always consistent across studies, as bacterial response can vary depending on nanoparticle properties such as size, surface chemistry, and synthesis method (Menichetti *et al.,* 2023). In the present study, the greater susceptibility of P. aeruginosa may be the specific surface characteristics of the green-synthesized ZnO nanoparticles and their interaction with the bacterial envelope. The ROS generated by ZnO nanoparticles may induce oxidative damage to the outer membrane and increase membrane permeability, potentially weakening the LPS-associated barrier and facilitating subsequent interactions of ZnO nanoparticles and Zn^{2+} ions with cellular components (Sirelkhatim *et al.,* 2015 and Saddiqi *et al.,* 2018). In addition, phytochemicals derived from the Mentha extract and associated with the nanoparticles' surface may modify the surface chemistry of the ZnO nanoparticles and influence their interaction with bacterial membranes. These surface-associated compounds may contribute to membrane perturbation or facilitate nanoparticle-cell interactions, which could partly explain the greater susceptibility of P. aeruginosa observed in this study (Shakerdarabad *et al.,* 2024). Furthermore, oxidative stress and membrane perturbation may affect membrane-associated transport systems and potentially

interfere with efflux-mediated resistance mechanisms. However, because of LPS integrity, efflux-pump activity, and the contribution of individual Mentha phytochemicals were not directly investigated in the present study, these mechanisms should be considered plausible explanations rather than experimentally confirmed pathways (Lee *et al.,* 2014).Overall, the difference in susceptibility observed between S. aureus and P. aeruginosa is best understood as the result of multiple interacting factors, including bacterial cell structure and nanoparticle characteristics, rather than a fixed rule related to Gram classification alone (Saed *et al.,* 2024). From a materials-engineering perspective, reducing nanoparticle agglomeration could improve the biological performance of the synthesized ZnO NPs (Sirelkhatim *et al.,* 2015). Future optimization of the calcination temperature and duration may help control particle growth and minimize sintering, while optimization of the capping conditions or the use of suitable stabilizing phytochemicals during synthesis may improve particle dispersion (Basnet *et al.,* 2018; Ismail *et al.,* 2019). Such optimization could increase the accessible surface area and facilitate greater nanoparticle-bacteria interaction and Zn^{2+} release, potentially enhancing the antibacterial activity (Mendes *et al.,* 2022). Furthermore, when compared with conventional standard therapeutics, the highest concentration of the green-synthesized ZnO NPs (50%) demonstrated superior antibacterial activity against P. aeruginosa (32.67 ± 0.58 mm) relative to the standard antibiotic piperacillin/tazobactam (17.33 ± 0.58 mm). Conversely, the positive control gentamicin retained a higher inhibition zone against S. aureus (32.33 ± 0.58 mm) compared to the 50% ZnO NP formulation (22.67 ± 0.58 mm). Meanwhile, the negative control (sterile distilled water) confirmed the validity of the assay by demonstrating no antibacterial activity (0.00 ± 0.00 mm) against both strains. These comparative findings underscore that while standard antibiotics remain potent against specific organisms, green-synthesized ZnO NPs serve as a highly effective broad-spectrum alternative agent, particularly against opportunistic Gram-negative strains such as Pseudomonas aeruginosa (Sirelkhatim *et al.,* 2015; Mendes *et al.,* 2022).

CONCLUSION

In this study, the ZnO NPs were successfully synthesized via a rapid, eco-friendly, and cost-effective green route using Mentha leaf extract as a natural reducing and capping agent. Comprehensive physicochemical characterization confirmed the formation of phase-pure crystalline ZnO with a hexagonal wurtzite structure (crystalline size of 24.04), as evidenced by the XRD, and demonstrated functional surface capping by Mentha-derived biomolecules via the FTIR. The SEM analysis revealed densely packed, quasi-spherical nanoparticle aggregates. The synthesized ZnO NPs exhibited potent, dose-dependent antibacterial activity against both Gram-positive (Staphylococcus aureus) and Gram-negative (Pseudomonas aeruginosa) pathogens, with notably higher susceptibility observed in Pseudomonas aeruginosa. At the highest concentration (50%), the ZnO NPs demonstrated superior antibacterial efficacy against Pseudomonas aeruginosa compared to the standard antibiotic piperacillin/tazobactam. While the present study offers valuable initial insights through the agar well diffusion assay, it was conducted as a preliminary investigation. Consequently, determination of the minimum inhibitory concentration and minimum bacterial concentration was beyond the scope of this work. To address this limitation, future research should incorporate broth microdilution assays to determine quantitative minimum inhibitory concentration and minimum bacterial concentration values, alongside optimization of calcination and capping parameters to minimize nanoparticle agglomeration, thereby maximizing their intrinsic biological potential for clinical and environmental applications.

REFERENCES

[1] Ahmed, B., Solanki, B., Zaidi, A., Khan, M. S., and Musarrat, J., Bacterial toxicity of biomimetic green zinc oxide nanoantibiotic: insights into ZnONP uptake and nanocolloid–bacteria interface, Toxicol. Res., 8, 246–261 (2019). https://doi.org/10.1039/c8tx00267c.

[2] A lavi, M., Dehestaniathar, S., Mohammadi, S., Maleki, A. & Karimi, N. (2021) 'Antibacterial Activities of Phytofabricated ZnO and CuO NPs by Mentha pulegium Leaf/Flower Mixture Extract against Antibiotic Resistant Bacteria', Avicenna Journal of Pharmaceutical Research, 11(3), pp. 497–504. https://pmc.ncbi.nlm.nih.gov/articles/PMC8421631/.

[3] A l-Darwesh, M.Y., Ibrahim, S.S. and Mohammed, M.A., A review on plant extract mediated green synthesis of zinc oxide nanoparticles and their biomedical applications, Results in Chemistry, 7, Article 101368 (2024). https://doi.org/10.1016/j.rechem.2024.101368.

[4] Al Sharif, R., Ayesh, A.S., Esaifan, M., Mazahrih, N., Bani Hani, N., Al Rjoub, B., et al., Green-synthesized zinc oxide nanoparticles with enhanced release behavior for sustainable agricultural applications, Solids, 6(4), Article 59 (2025). https://doi.org/10.3390/solids6040059.

[5] Alden, M. A. and Yaaqoob, L. A., Evaluation of the biological effect synthesized zinc oxide nanoparticles on Pseudomonas aeruginosa, Iraqi J. Agric. Sci., 53(1), 27–37 (2022). https://doi.org/10.36103/ijas.v53i1.1502.

[6] Ali, A., Zhang, N. and Santos, R. M., Mineral characterization using scanning electron microscopy (SEM): a review of the fundamentals, advancements, and research directions, Appl. Sci., 13(23), 12600 (2023). https://doi.org/10.3390/app132312600.

[7] Anik, A. B., Akash, M. H., Alam, M. A., Alam, M. Z., Sarker, D. and Sultana, N., Green synthesis of ZnO nanoparticles using Justicia adhatoda for effective photocatalytic degradation of methylene blue dye, RSC Advances, vol. 15, no. 54, 45874–45888 (2025). https://doi.org/10.1039/D5RA04295A.

[8] Arafah, M. W., Almutairi, B., Al-Zharani, M., Alkahtane, A. A., Al-Otibi, F. O., Ali, D., … and Alkahtani, S., The protective effect of Ammi visnaga extract against human hepatic cancer, J. King Saud Univ. Sci., 33(6), 101540 (2021). https://doi.org/10.1016/j.jksus.2021.101540.

[9] Arat, K. T., Fan Dong, X., Stühn, L., Neils, W. K. and Spagna, S., Nanoparticle characterization with in situ AFM-SEM-EDS, Microsc. Microanal., 30(Suppl 1), 499–501 (2024). https://doi.org/10.1093/mam/ozae044.233.

[10] Babaei, E. and Bazyari, A., Effects of drying conditions on physicochemical properties of epoxide sol–gel derived α-Fe_2O_3 and NiO: a comparison between xerogels and aerogels, Ceram. Int., 48(22), 33340–33349 (2022). https://doi.org/10.1016/j.ceramint.2022.07.XXX.

[11] Balouiri, M., Sadiki, M. and Ibnsouda, S. K., Methods for in vitro evaluating antimicrobial activity: A review, Journal of Pharmaceutical Analysis, vol. 6, no. 2, 71–79 (2016). https://doi.org/10.1016/j.jpha.2015.11.005.

[12] Baruah, J., Singh, L. S., Salvia, T. and Sarma, J., Antimicrobial resistance a continued global threat to public health–A perspective and mitigation strategies, J. Lab. Physicians, 16(4), 429-440 (2024). https://doi.org/10.25259/JLP_24_2024.

[13] Bisht, B. S., Karki, G., and Khati, P. S., Green Synthesis and Characterization of ZnO Nanoparticles from Water Extract of Chenopodium ambrosioides and Angelica glauca: A Comparative Analysis, J. Water Environ. Nanotechnol., 9(4), 449-457 (2024). https://doi.org/10.22090/jwent.2024.04.06.

[14] Basnet, P., Chanu, T. I., Samanta, D., and Chatterjee, S., A review on bio-synthesized zinc oxide nanoparticles using plant extracts as reductants and stabilizing agents, J. Photochem. Photobiol. B Biol., 183, 201–221 (2018). Basnet, P., Chanu, T. I., Samanta, D., and Chatterjee, S., A review on bio-synthesized zinc oxide nanoparticles using plant extracts as reductants and stabilizing agents, J. Photochem. Photobiol. B Biol., 183, 201–221 (2018). 10.1016/j.jphotobiol.2018.04.036.

[15] Chen, Z. Y., Shao, W. Z., Li, W. J., Sun, X. Y., Zhen, L. and Li, Y., Suppressing the agglomeration of ZnO nanoparticles in air by doping with lower electronegativity metallic ions: implications for Ag/ZnO electrical contact composites, ACS Applied Nano Materials, 5(8), 10809–10817 (2022). https://doi.org/10.1021/acsanm.2c0212.

[16] Dai, F., Zhuang, Q., Huang, G., Deng, H. and Zhang, X., Infrared spectrum characteristics and quantification of OH groups in coal, ACS Omega, vol. 8, no. 19, 17064–17076 (2023). https://doi.org/10.1021/acsomega.3c01178.

[17] Dar, N. A., Dar, P. A., Qadir, M. and Shah, W. A., Green synthesis and characterization of bioactive silver nanoparticles from Stachys tibetica, Sci. Rep., 15(1), 29673 (2025). https://doi.org/10.1038/s41598-025-92507-6.

[18] Davati, N. and Ghorbani, A., Comparison of the antibiotic resistance mechanisms in a gram-positive and a gram-negative bacterium by gene networks analysis, PLoS One, 19(11), e0311434 (2024). https://doi.org/10.1371/journal.pone.0311434.

[19] Debnath, G. H. and Mukherjee, P., Infrared absorption spectroscopy: A multifaceted characterization tool for nanomaterials, Langmuir, vol. 42, no. 5, 3703–3715 (2026). https://doi.org/10.1021/acs.langmuir.5c04282.

[20] Dong, L., Liu, Y. C., Tong, Y. H., Xiao, Z. Y., Zhang, J. Y., Lu, Y. M., Shen, D. Z. and Fan, X. W., Preparation of ZnO colloids by aggregation of the nanocrystal subunits, J. Colloid Interface Sci., 283(2), 380-384 (2005). https://doi.org/10.1016/j.jcis.2004.09.044.

[21] Duque-Sanchez, L., Pasic, P. J., Esneau, C., Batra, V., Tjandaputra, G., Tan, T., et al., Synergistic polymer coatings with antibacterial and antiviral properties for healthcare applications, ACS Omega, vol. 9, no. 30, 32662–32673 (2024). https://doi.org/10.1021/acsomega.4c03592.

[22] Dutta, R. K., Nenavathu, B. P., Gangishetty, M. K. and Reddy, A. V. R., Studies on antibacterial activity of ZnO nanoparticles by ROS induced lipid peroxidation, Colloids Surf. B Biointerfaces, 94, 143–150 (2012). https://doi.org/10.1016/j.colsurfb.2012.01.055.

[23] El Faroudi, L., Saadi, L., Barakat, A., Mansori, M., Abdelouahdi, K. and Solhy, A., Facile and sustainable synthesis of ZnO nanoparticles: effect of gelling agents on ZnO shapes and their photocatalytic performance, ACS Omega, 8(28), 24952–24963 (2023). https://doi.org/10.1021/acsomega.3c01491.

[24] El-Saadony, M. T., Fang, G., Yan, S., Alkafaas, S. S., El Nasharty, M. A., Khedr, S. A., … and AbuQamar, S. F., Green synthesis of zinc oxide nanoparticles: Preparation, characterization, and biomedical applications – A review, Int. J. Nanomedicine, 19, 12889-12937 (2024). https://doi.org/10.2147/IJN.S481472.

[25] Galvão, J. A., Miller, F. A., Ellet, C. and Anantheswaran, R. C., Modeling the development of inhibition zones in an agar diffusion bioassay, Food Science and Nutrition, 3(5), 394–403 (2015). https://doi.org/10.1002/fsn3.232.

[26] Hsiao, K. Y., Chung, R. J., Chang, P. P. and Tsai, T. H., Identification of hydroxyl and polysiloxane compounds via infrared absorption spectroscopy with targeted noise analysis, Polymers, vol. 17, no. 11, article 1533 (2025). https://doi.org/10.3390/polym17111533.

[27] Ilett, M., Matar, O., Bamiduro, F. et al., Nanoparticle corona artefacts derived from specimen preparation of particle suspensions, Sci. Rep., 10(1), 5278, 1–12 (2020). https://doi.org/10.1038/s41598-020-62253-y.

[28] Ismail, A. M., Menazea, A. A., Kabary, H. A., El-Sherbiny, A. E., and Samy, A., The influence of calcination temperature on structural and antimicrobial characteristics of zinc oxide nanoparticles synthesized by Sol–Gel method, J. Mol. Struct., 1196, 332–337 (2019). https://doi.org/10.1016/j.molstruc.2019.06.084.

[29] Jabeen, S., Facile Green Synthesis of Silver Doped ZnO Nanoparticles Using Tridax procumbens Leaf Extract and Their Evaluation of Antibacterial Activity, J. Water Environ. Nanotechnol., 5(4), 307-320 (2020). https://doi.org/10.22090/jwent.2020.04.002.

[30] Jiang, S., Lin, K. and Cai, M., ZnO nanomaterials: current advancements in antibacterial mechanisms and applications, Front. Chem., 8, 580 (2020). https://doi.org/10.3389/fchem.2020.00580.

[31] Kamal, A., Akhtar, M. S., Nazish, M., Tahira, K. T., Rahman, K. U., Iqbal, A., … and Zaman, W., Plant phytochemicals-mediated synthesis of zinc oxide nanoparticles with antimicrobial, pharmacological, and environmental applications, An. Acad. Bras. Cienc., 96(4), e20240436 (2024). https://doi.org/10.1590/0001-3765202420240436.

[32] Khorsand Zak, A. and Hashim, A. M., Advanced XRD peak broadening analysis of gallium-doped ZnO nanoparticles for crystallite size evaluation, Scientific Reports, vol. 16, article 1717 (2026). https://doi.org/10.1038/s41598-025-31317-2.

[33] Kuryliszyn-Kudelska, I. and Dobrowolski, W. D., Transition metal-doped ZnO and ZrO_2 nanocrystals: Correlations between structure, magnetism, and vibrational properties—A review, Applied Sciences, vol. 16, no. 2, article 786 (2026). https://doi.org/10.3390/app16020786.

[34] Laskar, I., and Saha, R., Synthesis and Characterization of Aluminium Oxide Nanoparticles Using Orange Peel Extract for Antibacterial and Antioxidant Activity, J. Water Environ. Nanotechnol., 10(4), 464-478 (2025). https://doi.org/10.22090/jwent.2025.04.008.

[35] Lee, J. H., Kim, Y. G., Cho, M. H., and Lee, J., ZnO nanoparticles inhibit Pseudomonas aeruginosa biofilm formation and virulence factor production, Microbiol. Res., 169, 888–896 (2014). https://doi.org/10.1016/j.micres.2014.05.005.

[36] Lee, J., Nakouzi, E., Heo, J., Legg, B. A., Schenter, G. K., Li, D., … Chun, J. (2023). Effects of particle shape and surface roughness on van der Waals interactions and coupling to dynamics in nanocrystals. Journal of Colloid and Interface Science, 652(Pt B), 1974–1983. https://doi.org/10.1016/j.jcis.2023.08.160.

[37] Lallo da Silva, B., Abuçafy, M. P., Berbel Manaia, E., Oshiro Junior, J. A., Chiari-Andréo, B. G., Pietro, R. C. L. R., and Chiavacci, L. A., Relationship between structure and antimicrobial activity of zinc oxide nanoparticles: An overview, Int. J. Nanomed., 14, 9395–9410 (2019). https://doi.org/10.2147/IJN.S216204.

[38] M utukwa, D., Taziwa, R.T. and Khotseng, L., A review of plant-mediated ZnO nanoparticles for photodegradation and antibacterial applications, Nanomaterials, 14(14), Article 1182 (2024). https://doi.org/10.3390/nano14141182.

[39] Mansy, S., Musleh, H., Shaat, S., Asad, J. and AlDahoudi, N., Computational and experimental study of wurtzite phase ZnO nanoparticles, Materials Today Communications, vol. 35, article 105688 (2023). https://doi.org/10.1016/j.mtcomm.2023.105688.

[40] Mazumder, J.A., Ahmad, A., Ali, J., Noori, R., Bhuyan, T., Sardar, M. and Sheehan, D., Biomimetic green synthesis of ZnO nanoflowers using α-amylase: from antimicrobial to toxicological evaluation, Scientific Reports, 14(1), Article 16566 (2024). https://doi.org/10.1038/s41598-024-67116-2.

[41] Mendes, C. R., Dilarri, G., Forsan, C. F., Sapata, V. M. R., Lopes, P. R. M., de Moraes, P. B., Montagnolli, R. N., Ferreira, H., and Bidoia, E. D., Antibacterial action and target mechanisms of zinc oxide nanoparticles against bacterial pathogens, Sci. Rep., 12, 2658 (2022). https://doi.org/10.1038/s41598-022-06657-y.

[42] Menichetti, A., Mavridi-Printezi, A., Mordini, D. and Montalti, M., Effect of size, shape and surface functionalization on the antibacterial activity of silver nanoparticles, J. Funct. Biomater., 14(5), 244 (2023). https://doi.org/10.3390/jfb14050244.

[43] Nan, J., Chu, Y., Guo, R. and Chen, P., Research on the antibacterial properties of nanoscale zinc oxide particles: Comprehensive review, Front. Mater., 11, 1449614 (2024). https://doi.org/10.3389/fmats.2024.1449614.

[44] Nasir, M., Naeem, A., Khan, L. Z., Zaib, N., Khan, H., Najam, Z. and Gul, A., Green synthesis of ZnO nanoparticles from melon peel and mint stem: antibacterial, antioxidant, and dye degradation potential, Sci. Rep., 16, Article number 16320 (2026). https://doi.org/10.1038/s41598-026-47322-y.

[45] Nguyen, V. T., Pham, N. H. and Papavassiliou, D. V., Aggregation of nanoparticles and morphology of aggregates in porous media with computations, J. Colloid Interface Sci., 650, 381–395 (2023).

[46] Rad, S. S., Sani, A. M. and Mohseni, S., Biosynthesis, characterization and antimicrobial activities of zinc oxide nanoparticles from leaf extract of Mentha pulegium (L.), Microbial Pathogenesis, 131, 239–245 (2019). https://doi.org/10.1016/j.micpath.2019.04.022.

[47] Rajalakshmi, S., Vijayakumar, S., Anupriya, A., Suganthy, N. and Devadharshini, D. (2026) 'Sustainable green synthesis of ZnO nanoparticles for antimicrobial and anticancer applications', Biochemical and Biophysical Research Communications, 817, p. 153721. https://doi.org/10.1016/j.bbrc.2026.153721.

[48] Riahi, S., Moussa, N. B., Lajnef, M., Jebari, N., Dabek, A., Chtourou, R., … and Herth, E., Bactericidal activity of ZnO nanoparticles against multidrug-resistant bacteria, J. Mol. Liq., 387, 122596 (2023). https://doi.org/10.1016/j.molliq.2023.122596.

[49] Saed, M., Ayivi, R. D., Wei, J. and Obare, S. O., Gold nanoparticles antibacterial activity: Does the surface matter?, Colloid Interface Sci. Commun., 62, 100804 (2024). https://doi.org/10.1016/j.colcom.2024.100804.

[50] Sahithya, K., Mouli, T., Devika, P. R., and Harshitha, C. K., Antimicrobial and Environmental Applications of Inorganic Nanoparticles Synthesised from Plants, J. Water Environ. Nanotechnol., 7(4), 389-406 (2022). https://doi.org/10.22090/jwent.2022.04.006.

[51] Sanders, E. R., Aseptic laboratory techniques: plating methods, Journal of Visualized Experiments (JoVE), no. 63, article e3064 (2012). https://doi.org/10.3791/3064.

[52] Sharma, S. K., Kumar, R., Vaishnav, A., Sharma, P. K., Singh, U. B. and Sharma, A. K., Microbial cultures: maintenance, preservation and registration, in Modern Tools and Techniques to Understand Microbes, Springer International Publishing, Cham, pp. 335–367 (2017). https://doi.org/10.1007/978-3-319-49197-4_22.

[53] Shakerdarabad, R., Mohabatkar, H., Behbahani, M., and Dini, G., Antibiofilm and antibacterial activities of green synthesized ZnO nanoparticles against Erwinia amylovora and Pseudomonas syringae pv. syringae: in vitro and in silico investigations, Microb. Pathog., 196, 107011 (2024). https://doi.org/10.1016/j.micpath.2024.107011.

[54] Shukla, U., Fourier transform infrared spectroscopy: A powerful method for creating fingerprint of molecules of nanomaterials, Journal of Molecular Structure, vol. 1322, article 140454 (2025). https://doi.org/10.1016/j.molstruc.2025.140454.

[55] Siddiqi, K. S., Ur Rahman, A., Tajuddin, and Husen, A., Properties of zinc oxide nanoparticles and their activity against microbes, Nanoscale Res. Lett., 13, 141 (2018). https://doi.org/10.1186/s11671-018-2532-3.

[56] Sirelkhatim, A., Mahmud, S., Seeni, A., Kaus, N. H. M., Ann, L. C., Bakhori, S. K. M., Hasan, H., and Mohamad, D., Review on zinc oxide nanoparticles: Antibacterial activity and toxicity mechanism, Nano-Micro Lett., 7, 219–242 (2015). https://doi.org/10.1007/s40820-015-0040-x.

[57] Talukdar, P. J., Bharti, K., Banerjee, S., Basu, S., Das, S. K., Paul, R. R., et al., A comprehensive FTIR micro-spectroscopic analysis and classification of precancerous human oral tissue aided by machine learning, Sensors & Diagnostics, vol. 3, no. 11, 1854–1865 (2024). https://doi.org/10.1039/D4SD00223A.

[58] Tran, X. T., Bien, T. T. L., Van Tran, T. and Nguyen, T. T. T., Biosynthesis of ZnO nanoparticles using aqueous extracts of Eclipta prostrata and Piper longum: Characterization and assessment of their antioxidant, antibacterial, and photocatalytic properties, Nanoscale Advances, vol. 6, no. 19, 4885–4899 (2024). https://doi.org/10.1039/D4NA00387H.

[59] U dayagiri, H., Sana, S.S., Dogiparthi, L.K., Vadde, R., Varma, R.S., Koduru, J.R., et al., Phytochemical fabrication of ZnO nanoparticles and their antibacterial and anti-biofilm activity, Scientific Reports, 14(1), Article 19714 (2024). https://doi.org/10.1038/s41598-024-70783-4.

[60] V itasovic, T., Caniglia, G., Eghtesadi, N., Ceccato, M., Bojesen, E. D., Gosewinkel, U., et al. Antibacterial action of Zn^{2+} ions driven by the in vivo formed ZnO nanoparticles, ACS Applied Materials & Interfaces, 16(24), 30847–30859 (2024). https://doi.org/10.1021/acsami.4c04682.

[61] Verma, L. M., Kumar, A., Bashir, A. U., Gangwar, U., Ingole, P. P. and Sharma, S., Phase controlled green synthesis of wurtzite (P63mc) ZnO nanoparticles: interplay of green ligands with precursor anions, anisotropy and photocatalysis, Nanoscale Adv., 6(1), 155-169 (2024). https://doi.org/10.1039/D3NA00596H.

[62] Wicks, J. H., Nelson, R. L. and Krejcarek, G. E., Rapid inoculum standardization system: a novel device for standardization of inocula in antimicrobial susceptibility testing, Journal of Clinical Microbiology, vol. 17, no. 6, 1114–1119 (1983). https://doi.org/10.1128/JCM.17.6.1114-1119.1983.

[63] Wu, W., Huang, J. and Xu, Z., Antibiotic influx and efflux in Pseudomonas aeruginosa: Regulation and therapeutic implications, Microb. Biotechnol., 17(5), e14487 (2024). https://doi.org/10.1111/1751-7915.14487.

[64] Xie, J., Feng, K., Ye, R., Wang, M., Wang, Y., Fan, X. and Liu, R., Controlled synthesis and formation mechanism of uniformly sized spherical CeO_2 nanoparticles, Materials, vol. 19, no. 1, article 211 (2026). https://doi.org/10.3390/ma19010211.

[65] Xu, F., Xie, Y., Yu, W. and Wang, Z., Breaking the outer membrane barrier: structure, targets, and antimicrobial strategies for Gram-negative bacteria, Front. Microbiol., 17, 1734749 (2026). https://doi.org/10.3389/fmicb.2026.1734749.

[66] Xu, J., Huang, Y., Zhu, S., Abbes, N., Jing, X. and Zhang, L., A review of the green synthesis of ZnO nanoparticles using plant extracts and their prospects for application in antibacterial textiles, Journal of Engineered Fibers and Fabrics, 16, Article 15589250211046242 (2021). https://doi.org/10.1177/15589250211046242.

[67] Zak, A. K., Esmaeilzadeh, J. and Hashim, A. M., X-ray peak broadening and strain-driven preferred orientations of pure and Al-doped ZnO nanoparticles prepared by a green gelatin-based sol-gel method, Journal of Molecular Structure, vol. 1303, article 137537 (2024). https://doi.org/10.1016/j.molstruc.2024.137537.

[68] Zeghoud, S., Hemmami, H., Seghir, B.B., Amor, I.B., Kouadri, I., Rebiai, A., et al., A review on biogenic green synthesis of ZnO nanoparticles by plant biomass and their applications, Materials Today Communications, 33, Article 104747 (2022). https://doi.org/10.1016/j.mtcomm.2022.104747.

[69] Zubair, N., Al-Oqaili, R. M. S., Yousaf, M. J., Siddique, A., Awwad, F. A., Ismail, E. A., … and Timraz, J. H., Morphology dependent antibacterial activity of zinc oxide nanoparticles against clinically relevant bacteria, Sci. Rep., 15, 10381 (2025). https://doi.org/10.1038/s41598-025-94458-9.